A model based on adipose and muscle-related indicators evaluated by CT images for predicting microvascular invasion in HCC patients

Xin-Cheng Mao[1], Shuo Shi[2], Lun-Jie Yan[1], Han-Chao Wang[3], Zi-Niu Ding[1], Hui Liu[1], Guo-Qiang Pan[1], Xiao Zhang[1], Cheng-Long Han[1], Bao-Wen Tian[1], Dong-Xu Wang[1], Si-Yu Tan[1], Zhao-Ru Dong[1], Yu-Chuan Yan[1] and Tao Li[1*]

Abstract

Background and aim The presence of microvascular invasion (MVI) will impair the surgical outcome of hepatocellular carcinoma (HCC). Adipose and muscle tissues have been confirmed to be associated with the prognosis of HCC. We aimed to develop and validate a nomogram based on adipose and muscle related-variables for preoperative prediction of MVI in HCC.

Methods One hundred fifty-eight HCC patients from institution A (training cohort) and 53 HCC patients from institution B (validation cohort) were included, all of whom underwent preoperative CT scan and curative resection with confirmed pathological diagnoses. Least absolute shrinkage and selection operator (LASSO) logistic regression was applied to data dimensionality reduction and screening. Nomogram was constructed based on the independent variables, and evaluated by external validation, calibration curve, receiver operating characteristic (ROC) curve and decision curve analysis (DCA).

Results Histopathologically identified MVI was found in 101 of 211 patients (47.9%). The preoperative imaging and clinical variables associated with MVI were visceral adipose tissue (VAT) density, intramuscular adipose tissue index (IMATI), skeletal muscle (SM) area, age, tumor size and cirrhosis. Incorporating these 6 factors, the nomogram achieved good concordance index of 0.79 (95%CI: 0.72–0.86) and 0.75 (95%CI: 0.62–0.89) in training and validation cohorts, respectively. In addition, calibration curve exhibited good consistency between predicted and actual MVI probabilities. ROC curve and DCA of the nomogram showed superior performance than that of models only depended on clinical or imaging variables. Based on the nomogram score, patients were divided into high (> 273.8) and low (< = 273.8) risk of MVI presence groups. For patients with high MVI risk, wide-margin resection or anatomical resection could significantly improve the 2-year recurrence free survival.

Conclusion By combining 6 preoperative independently predictive factors of MVI, a nomogram was constructed. This model provides an optimal preoperative estimation of MVI risk in HCC patients, and may help to stratify high-risk individuals and optimize clinical decision making.

*Correspondence:
Tao Li
litao7706@163.com
Full list of author information is available at the end of the article

Mao *et al. Biomarker Research*   (2023) 11:87

Page 2 of 16

Introduction

Hepatocellular carcinoma (HCC) represents the most frequent type of primary liver cancer and ranks as the third leading cause of cancer-related death worldwide [1]. Surgical resection is the backbone of curative treatment for HCC. Although the surgical operation of HCC has been extremely developed, the prognosis of HCC is still very poor [2]. The recurrence after operation remains a major obstacle to improve survival and the 5-year recurrence rates are up to 70%, even in patients with single small HCC (≤ 2 cm) [3]. One of the main reasons is microvascular invasion (MVI). MVI, a histopathological feature of micro-metastases, can be observed in 15.0%-57.1% of surgical specimens and stands as a key predictor for early recurrence and poor prognosis [4, 5]. In addition, the presence of MVI has been an essential factor influencing the long-term prognosis of HCC patients underwent liver transplantation [6]. However, the impact of MVI has largely been disregarded by clinicians as it can only be found by histologic examination of postoperative specimens. As MVI represents an aggressive behavior of HCC [5], individualized surgical management for patients should be formulated according to the risk–benefit assessment of MVI before surgery. For patients with high risk of MVI, anatomical subsegmentectomy or partial hepatectomy with wide margin is recommended under better liver function, which could decrease the risk of recurrence [7]. Therefore, establishing a highly accurate risk model for predicting MVI can help to stratify high-risk individuals, optimize clinical decision making and improve prognosis.

Over the last decades, numerous efforts have been taken to estimate MVI prior to surgery. Cucchetti et al. utilized four clinical common variables, including alpha-fetoprotein (AFP), tumor number, size and volume, to develop an artificial neural network (ANN) model that accurately identified 91% of MVI cases in testing group [8]. However, this ANN model requires specialized computer software, which potentially limits its utility in routine clinical application. In contrast, the nomogram might be a convenient option and provide highly accurate and individualized risk estimate [9]. For hepatitis B virus–related HCC patients, Li et al. constructed a nomogram by incorporating contrast-enhanced magnetic resonance imaging (MRI) data with hematology data, which achieved relatively good predictive accuracy for MVI [10]. Unfortunately, serum biomarkers might also have abnormally change in non-cancerous liver lesions, so specificity is not optimal. As technologies advance, radiomics nomograms based on contrast-enhanced computed tomography (CT) or gadoxetic acid-enhanced MRI have achieved excellent concordance indexes (C indexes) in predicting MVI [11, 12]. However, random split sample approach was used in these studies to generate training and validation sets. Although this method is commonly used, it represents an inefficient use of the data and has large variability, especially in condition of small population [13]. In addition, the number of candidates radiomic features is orders of magnitude higher than the number of cases, which could lead to overfitting errors [14]. Taken together, it is necessary to identify novel predictors and employ appropriate statistical method to construct a nomogram for predicting MVI before surgery.

Recently, the impact of body composition changes, which mainly encompasses adipose and muscle tissues, on the prognosis of HCC has received wide attention [15–20]. Skeletal muscle index (SMI) [15, 20], subcutaneous adipose tissue index (SATI) [16, 18] and visceral adipose tissue index (VATI) [19, 20] have been recognized as strongly correlated variables with the occurrence and development of HCC. Some of them act as negative factors by increasing inflammatory response, altering the hormonal level or disrupting the balance between anabolic and catabolic metabolisms [21, 22], while others act as protective factors by stimulating the insulin response, boosting lipid metabolism or enhancing immune function [16]. Therefore, it's speculated that the changes of adipose and muscle tissues may have some correlation with the presence of MVI in HCC patients. In fact, Arsenii et al. [23] and Wu et al. [24] have performed relevant studies. Despite their efforts, these studies lacked sufficient evidence, as the former did not yield any positive results, while the latter only proved the correlation of SAT and VAT with the presence of MVI in univariate logistic analysis. In this study, we aim to collect adipose and muscle related clinical variables of HCC patients to determine the variables that are most strongly associated with MVI, and construct a nomogram model to assist surgeons in risk stratification and personalized treatment.

Methods

Study population

Between January 01, 2018, and December 31, 2021, retrospective data on patients diagnosed with HCC through postoperative pathology were collected at Qilu

Mao *et al. Biomarker Research*   (2023) 11:87

Page 3 of 16

hospital of Shandong university (institution A) and the Second Hospital of Shandong University (institution B). This retrospective study was reviewed and approved by Institutional Review Board of Qilu hospital of Shandong university [approval number: 2021(222)].

Inclusion criteria were as follows: 1) liver resection was the initial treatment, and patients received no preoperative treatment, such as transcatheter arterial chemoembolization (TACE), targeted immunotherapy, or radiotherapy; 2) the diagnosis of MVI was confirmed by pathological examination; 3) complete clinical data can be acquired from electronic medical record, and CT scan of the abdomen was performed within two weeks before surgery in these two hospitals. Patients with a history of other malignancies, suboptimal CT images, absence of MVI condition in pathology reports were excluded. The detailed screening procedure was shown in Fig. 1.

Clinical data and follow-up

Clinical data included the MVI status (negative vs. positive), age (<60 vs. ≥ 60 years), sex (female vs. male), tumor size (<5 vs. ≥ 5 cm), Child–Pugh class (A vs. B), cirrhosis (no vs. yes), hepatitis B surface antigen (HBsAg) status (negative vs. positive), albumin (ALB, <3.5 vs. ≥ 3.5 g/dL), alpha fetoprotein (AFP, <400 vs. ≥ 400 ng/mL), aspartate transaminase (AST, <40 vs. ≥ 40 U/L) level, alanine aminotransferase (ALT, <44 vs. ≥ 44 U/L) level, total bilirubin (TB, <17.1 vs. ≥ 17.1 μmol/L) level, body mass index (BMI, <24.9 vs. ≥ 24.9 kg/m^2), surgical approach (open laparotomy vs. laparoscopic), resection method (non-anatomical vs. anatomical), and surgical margin (<1 vs. ≥ 1 cm). The definition of surgical margin was the shortest distance from the edge of the tumor to the resection line. MVI is defined as the presence of cancer cell clusters within the lumen of blood vessels lined by endothelial cells under a microscope [4]. As macrovascular wall contains layers of smooth muscle or elastic
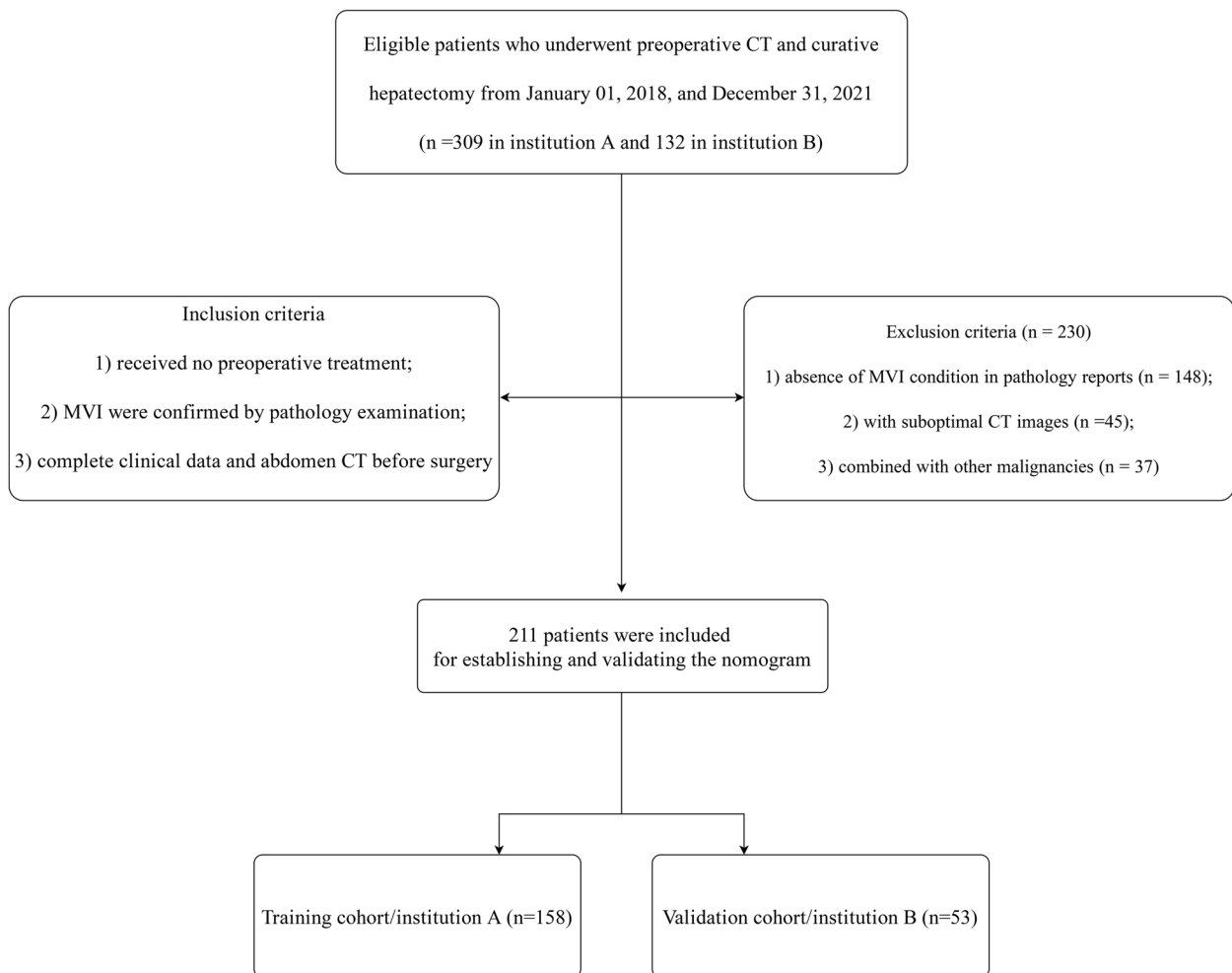

Fig. 1 Flowchart of the included HCC patients

Mao *et al. Biomarker Research*   (2023) 11:87

Page 4 of 16

fibers, while microvascular wall typically consists only of endothelial cells. In order to help distinguish MVI from macrovascular invasion, immunohistochemistry was performed to examine the expression of CD34 (vascular endothelium), smooth muscle α-actin (vascular smooth muscle), and elastic fibers (elastic fiber layer of tiny blood vessel wall) [25].

All patients were recommended to surveillance every 3 months for the first 2 years and then every 6 months thereafter. Postoperative follow-up included abdominal ultrasound, CT or MRI, routine blood, serum biochemistry, and tumor-specific biomarkers. Early recurrence was defined as intrahepatic recurrence within two years after curative resection. Recurrence free survival (RFS) was defined as the duration from the data of surgery to either the date of tumor recurrence or the last follow-up. Overall survival (OS) was defined as the interval from the date of surgery to the date of death or the last follow-up.

CT-related body composition variables

Abdominal CT scan for included patients from these two hospitals were performed within two weeks before surgery using the equipment of Siemens 64-slice spiral CT scanner from the same manufacturer [26, 27] to avoid data heterogeneity resulting from CT equipment. Semi-automatic software (SliceOmatic™ version 5.0, Tomovision, Montreal, Quebec, Canada) was utilized to quantify the areas and density of skeletal muscle (SM) tissue and different adipose tissues [(i.e., subcutaneous adipose tissue (SAT), visceral adipose tissue (VAT) and intramuscular adipose tissue (IMAT)] in the single cross-sectional CT images at the central level of the third lumbar vertebra (L3). The areas quantified from the single cross-sectional CT image at the L3 level exhibited the highest correlation with the overall body tissue mass, demonstrating correlation coefficients (r^2) of 0.855 and 0.927 for muscle and adipose tissues, respectively [28]. The SM tissue at L3 level consisted of the psoas, quadratus lumborum, erector spinae, transversus abdominis, external and internal obliques, and rectus abdominis muscles. SM area referred the sum of cross-sectional areas of the aforementioned muscles, measured in centimeters squared (cm^2). Area of each adipose tissues also referred the cross-sectional area on the L3 level. The above each tissue areas were normalized by the heights squared (m^2) to obtain their corresponding indexes (cm^2/m^2), including SMI, SATI, VATI and IMAT index (IMATI). Density of muscle and adipose tissues referred the mean radiologic tissue attenuation for each type of tissue, measured in Hounsfield Unit (HU). The formula for calculating visceral to subcutaneous adipose tissue area ratio (VSR) was VAT area divided by SAT area. The specific steps to obtain body composition-related parameters were as

follows: Firstly, the radiodensity threshold-based technique of SliceOmatic™ was utilized to semi-automatically outline the initial delineations of the region of interest. The HU thresholds were applied as follows: -30 to 150 HU for SM, -190 to -30 HU for SAT and IMAT, and -150 to -30 HU for VAT [29, 30]. Then a clinician under the guidance of an experienced radiologist performed a manual inspection and adjustment of the region of interest without knowing the patients' characteristics and outcomes. Finally, the areas (cm^2) and density values (HU) were acquired to provide characterization for each body composition. Examples of delineation were shown in the Supplementary Fig. 1. The "SurvivalROC" package of R software was used to calculate the cut-off values for each variable. This package could repeatedly evaluate cut-off values obtained from receiver operating characteristic (ROC) curves and identified the optimal cut-off values based on the maximum log-rank statistic. Notably, cut-off values were also determined according to gender, as body compositions varied between genders. The detailed cut-off values were shown in Supplementary Table 1. To ensure the inter-reader consistency, two clinicians with more than 5 years' experience in hepatobiliary surgery independently completed the delineations of all variables. Then 40 pairs of samples were randomly selected for comparison and the inter-reader fluctuated between 0.87 and 0.91.

Statistical analysis

Chi-square test was utilized to compared the categorical variables, and results were presented as absolute counts and percentages format [No. (%)]. The process of data dimensionality reduction and screening was implemented by the least absolute shrinkage and selection operator (LASSO) regression analysis. Variables with non-zero coefficients were first included in univariate logistic regression analysis, and then all variables with *P*-values less than 0.1 were entered into multivariate stepwise forward regression analysis to identify independent variables with *P*-values less than 0.05. A nomogram was constructed using the independent predictors. To assess the predictive performance of the nomogram, we performed calibration curve and C index yielded by 1000 bootstrapping techniques. The clinical utility of nomogram was evaluated through comparing its ROC curve and decision curve analysis (DCA) with those of imaging and clinical model. In addition, we used 200 rounds of tenfold internal cross-validation and external validation methods to evaluate our nomogram. The MVI risk score for all patients was computed using the nomogram, followed by allocation of all patients into low and high-risk groups using the cut-off value with the highest Youden index (the sum of sensitivity and specificity). Finally, the

Mao *et al. Biomarker Research*   (2023) 11:87

Page 5 of 16

Kaplan–Meier (KM) method and the log-rank test were employed to generate survival curves for the purpose of stratifying risk factors and helping surgeons to make more personalized treatment plans. The above all statistical analyses were performed using and R software (version 4.0.2), with packages: "rms", "survival", "pROC", "caret", "rmda".

Results

Baseline characteristics of patients
During the study period, 158 HCC patients form institution A and 53 HCC patients form institution B met the inclusion criteria were enrolled. The former was the training cohort with the median follow-up time of 23.9 months, and the latter was the validation cohort with the median follow-up time of 27.1 months. Pathological confirmed MVI was found in 101 (47.9%) individuals of all patients. The detailed clinical, adipose as well as muscle related variables were shown in Table 1, respectively.

Data dimensionality reduction and screening
LASSO regression analysis was performed to identify the most crucial variables linked with the risk of MVI. To guarantee precision, the algorithm's iterations were set to 1000. In addition, cv.glmnet function was used to perform tenfold cross validation to diminish the possibility of overfitting. The distribution of LASSO regression coefficients and cross-validation plots were shown in Fig. 2. Dotted vertical lines indicated the value of lambda.min and lambda.1se. Finally, 18 variables (age, tumor size, CTP, cirrhosis, HBsAg, AFP, TB, resection method, SAT density, VAT area, VAT density, VATI, VSR, IMAT area, IMATI, SM area, SM density, SMI) with nonzero coefficients were selected according to the value of lambda. min ($\lambda = 0.03139931$).

Logistic regression analysis, construction, and validation of nomogram
The above 18 variables were subjected to univariate logistic analysis, and then 8 variables (age, tumor size, cirrhosis, VAT density, IMAT area, IMATI, SM area, SMI) with *P*-values of less than 0.1 were incorporated into multivariate analysis. Except for IMAT area and SMI, the remaining 6 variables [age (OR = 0.214; 95%CI = 0.088–0.522; *P* = 0.001), tumor size (OR = 2.359; 95%CI = 1.115–4.989; *P* = 0.025), cirrhosis (OR = 2.518; 95%CI = 1.077–5.887; *P* = 0.033), VAT density (OR = 3.468; 95%CI = 1.533–7.847; *P* = 0.003), IMATI (OR = 4.783; 95%CI = 2.058–11.112; *P* < 0.001), SM area (OR = 0.295; 95%CI = 0.120–0.725; *P* = 0.008)] were all significant independent predictors for MVI. The detailed data was shown in Table 2.

These Six independent predictors were utilized to form an MVI-predicting nomogram (Fig. 3a). The nomogram provided good accuracy in estimating the risk of MVI, with C index of 0.79 (95%CI: 0.72–0.86), R^2 of 0.35, discrimination index (D index) of 0.30, Brier score of 0.18, Emax of 0.05, Evag of 0.02 (Fig. 3b). Following 200 rounds of tenfold internal cross-validation, there was little variation in the values of the above variables (Table 3), with the correct C index of 0.79, R^2 of 0.32, D index of 0.24, Brier score of 0.18, Emax of 0.30, Evag of 0.13. In addition, calibration curve exhibited good consistency between predicted MVI probability of nomogram and the actual probability.

In validation cohort, the nomogram presented a C index of 0.75 (95%CI: 0.62–0.89) for the evaluation of risk associated with MVI. Moreover, the fitting calibration curve was acceptable (Fig. 3c).

Clinical utility of the nomogram
The independent predictors of MVI included three clinical variables (age, tumor size and cirrhosis) and three imaging variables (VAT density, IMATI and SM area). These clinical and imaging variables were used separately to construct new clinical and imaging model, which were then compared with this nomogram to verify its clinical utility. The ROC curve indicated that the discriminative ability of the nomogram in predicting MVI was better than that of the imaging and clinical models, with AUC values of 0.791, 0.711, 0.673 and 0.716, 0.654, 0.633 in training and validation cohorts, respectively (Fig. 4a, b). In addition, the DCA of nomogram also exhibited a wider range of threshold probabilities in comparison to the imaging and clinical model (Fig. 4c, d).

Risk stratification of MVI based on the nomogram and survival analysis
The optimal cut-off value of the nomogram scores in training cohort was determined to be 273.8, and the sensitivity and specificity for distinguishing the presence from absence of MVI according to this value were 79.7% and 63.3%, respectively (Supplementary Fig. 2). Based on the cut-off value, patients in two cohorts were divided into high (> 273.8) and low (< = 273.8) risk groups. Kaplan–Meier curves showed that in both training and validation cohorts, patients with high-risk of MVI had higher 2-year recurrence rate and shorter OS than patients with low-risk (Fig. 5). For patients with high MVI risk, wide-margin resection or anatomical resection could significantly improve the 2-year RFS, while only wide-margin resection could significantly improve the OS (Figs. 6 and 7). In contrast, for low-risk patients, neither surgical approaches, nor

Mao *et al. Biomarker Research*   (2023) 11:87

Page 6 of 16

Table 1 Baseline characteristics of HCC patients

Variable	Cohort, No. (%)			P value
	Overall (*n* = 211)	Training cohort (*n* = 158)	Validation cohort (*n* = 53)	
MVI				0.36
Negative	110 (52.1)	79 (50.0)	31 (58.5)	
Positive	101 (47.9)	79 (50.0)	22 (41.5)	
Sex				0.75
Female	41 (19.4)	32 (20.3)	9 (17.0)	
Male	170 (80.6)	126 (79.7)	44 (83.0)	
Age (years)				0.02
<60	118 (55.9)	96 (60.8)	22 (41.5)	
>=60	93 (44.1)	62 (39.2)	31 (58.5)	
Tumor size (cm)				0.05
<5	98 (46.4)	80 (50.6)	18 (34.0)	
>=5	113 (53.6)	78 (49.4)	35 (66.0)	
Child–Pugh class				0.99
A	201 (95.3)	150 (94.9)	51 (96.2)	
B	10 (4.7)	8 (5.1)	2 (3.8)	
Cirrhosis				0.96
No	69 (32.7)	51 (32.3)	18 (34.0)	
Yes	142 (67.3)	107 (67.7)	35 (66.0)	
HBsAg				0.34
Negative	44 (20.9)	30 (19.0)	14 (26.4)	
Positive	167 (79.1)	128 (81.0)	39 (73.6)	
Albumin (g/dL)				0.14
<3.5	13 (6.2)	7 (4.4)	6 (11.3)	
>=3.5	198 (93.8)	151 (95.6)	47 (88.7)	
AFP (ng/mL)				0.04
<400	150 (71.1)	106 (67.1)	44 (83.0)	
>=400	61 (28.9)	52 (32.9)	9 (17.0)	
AST (U/L)				0.75
<40	145 (68.7)	110 (69.6)	35 (66.0)	
>=40	66 (31.3)	48 (30.4)	18 (34.0)	
ALT (U/L)				1.00
<44	146 (69.2)	109 (69.0)	37 (69.8)	
>=44	65 (30.8)	49 (31.0)	16 (30.2)	
TB (umol/L)				1.00
<17.1	132 (62.6)	99 (62.7)	33 (62.3)	
>=17.1	79 (37.4)	59 (37.3)	20 (37.7)	
BMI (kg/m^2)				0.01
<24.9	162 (76.8)	135 (85.4)	27 (50.9)	
>=24.9	49 (23.2)	23 (14.6)	26 (49.1)	
Surgical approach				0.09
Open laparotomy	99 (46.9)	80 (50.6)	19 (35.8)	
Laparoscopic	112 (53.1)	78 (49.4)	34 (64.2)	
Resection method				1.00
Non-anatomical	97 (46.0)	73 (46.2)	24 (45.3)	
Anatomical	114 (54.0)	85 (53.8)	29 (54.7)	

Mao *et al. Biomarker Research*   (2023) 11:87

Page 7 of 16

Table 1 (continued)

Variable	Cohort, No. (%)			P value
	Overall (*n* = 211)	Training cohort (*n* = 158)	Validation cohort (*n* = 53)	
Surgical margin (cm)				0.03
< 1	150 (71.1)	119 (75.3)	31 (58.5)	
> = 1	61 (28.9)	39 (24.7)	22 (41.5)	
SAT area (cm^2)				1.00
Small	80 (37.9)	60 (38.0)	20 (37.7)	
Large	131 (62.1)	98 (62.0)	33 (62.3)	
SAT density (HU)				0.08
Low	119 (56.4)	95 (60.1)	24 (45.3)	
High	92 (43.6)	63 (39.9)	29 (54.7)	
SATI (cm^2/m^2)				0.27
Low	157 (74.4)	114 (72.2)	43 (81.1)	
High	54 (25.6)	44 (27.8)	10 (18.9)	
VAT area (cm^2)				0.14
Small	88 (41.7)	71 (44.9)	17 (32.1)	
Large	123 (58.3)	87 (55.1)	36 (67.9)	
VAT density (HU)				0.77
Low	90 (55.0)	66 (41.8)	24 (45.3)	
High	121 (45.0)	92 (58.2)	29 (54.7)	
VATI (cm^2/m^2)				0.10
Low	90 (42.7)	73 (46.2)	17 (32.1)	
High	121 (57.3)	85 (53.8)	36 (67.9)	
VSR				0.19
Low	90 (42.7)	72 (45.6)	18 (34.0)	
High	121 (57.3)	86 (54.4)	35 (66.0)	
IMAT area (cm^2)				1.00
Small	107 (50.7)	80 (50.6)	27 (50.9)	
Large	104 (49.3)	78 (49.4)	26 (49.1)	
IMAT density (HU)				0.19
Low	102 (48.3)	81 (51.3)	21 (39.6)	
High	109 (51.7)	77 (48.7)	32 (60.4)	
IMATI (cm^2/m^2)				1.00
Low	103 (48.8)	77 (48.7)	26 (49.1)	
High	108 (51.2)	81 (51.3)	27 (50.9)	
SM area (cm^2)				0.65
Small	63 (29.9)	49 (31.0)	14 (26.4)	
Large	148 (70.1)	109 (69.0)	39 (73.6)	
SM density (HU)				0.55
Low	118 (55.9)	86 (54.4)	32 (60.4)	
High	93 (44.1)	72 (45.6)	21 (39.6)	
SMI (cm^2/m^2)				0.40
Low	99 (46.9)	71 (44.9)	28 (52.8)	
High	112 (53.1)	87 (55.1)	25 (47.2)	

Abbreviations: *HCC* Hepatocellular carcinoma, *MVI* Microvascular invasion, *HBsAg* Hepatitis B surface Antigen, *AFP* Alpha fetoprotein, *AST* Aspartate aminotransferase, *ALT* Alanine aminotransferase, *TB* Total bilirubin, *BMI* Body mass index, *HU* Hounsfield Unit, *SAT* Subcutaneous adipose tissue, *SATI* Subcutaneous adipose tissue index, *VAT* Visceral adipose tissue, *VATI* Visceral adipose tissue index, *VSR* Visceral to subcutaneous adipose tissue area ratio, *IMAT* Intramuscular adipose tissue, *IMATI* Intramuscular adipose tissue index, *SM* Skeletal muscle, *SMI* Skeletal muscle index

Mao *et al. Biomarker Research*   (2023) 11:87
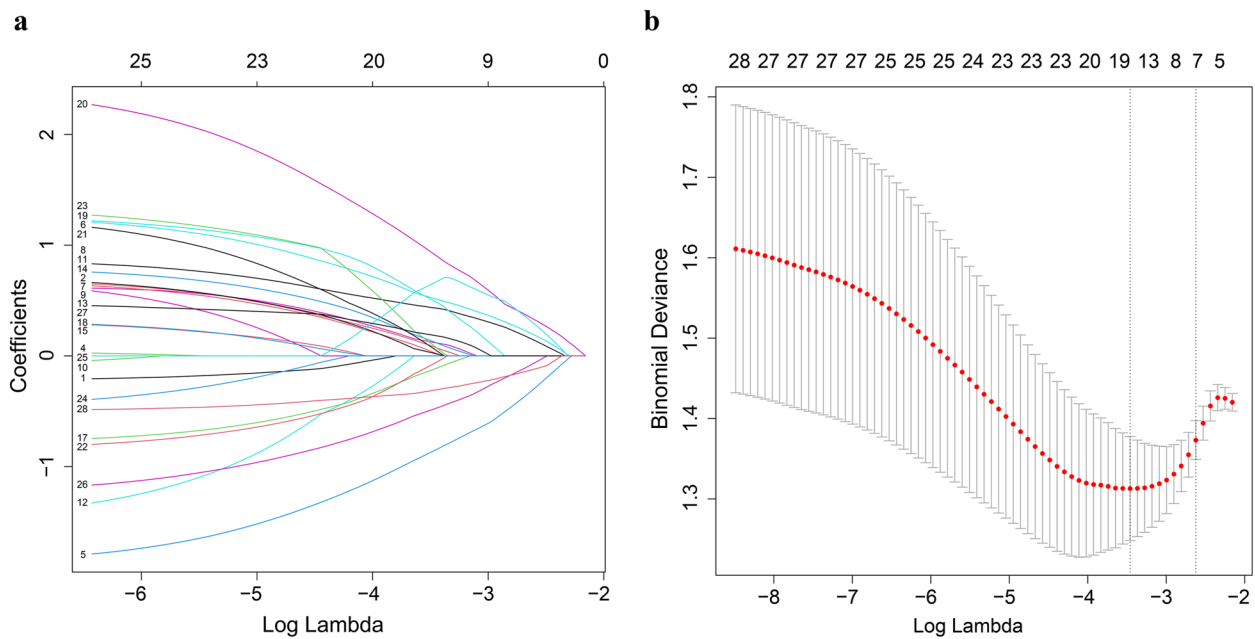
Page 8 of 16

Fig. 2 Selecting influence factors by using LASSO regression model. **a** LASSO coefficient curves for 28 predictors. **b** Identification of the best punishment coefficient lambda in LASSO regression model

Table 2 Univariate and multivariate logistic analysis of MVI presence for HCC patients

Variable	Univariate Analysis		Multivariable Analysis	
	OR (95% CI)	*P* value	OR (95% CI)	*P* value
Age, > =60 vs < 60	0.421 (0.216–0.806)	0.010	0.214 (0.088–0.522)	0.001
Tumor size, > =5 vs < 5, cm	2.274 (1.209–4.336)	0.011	2.359 (1.115–4.989)	0.025
Child–Pugh class, B vs A	3.164 (0.703–22.073)	0.167		
Cirrhosis, yes vs no	2.431 (1.231–4.921)	0.012	2.518 (1.077–5.887)	0.033
HBsAg, positive vs negative	1.958 (0.875–4.568)	0.108		
AFP, > =400 vs < 400, ng/mL	1.586 (0.815–3.124)	0.177		
TB, > =17.1 vs < 17.1, umol/L	1.311 (0.688–2.514)	0.411		
Resection method	1.430 (0.764–2.691)	0.265		
SAT density, high vs low	0.620 (0.324–1.175)	0.145		
VAT area, large vs small	1.432 (0.764–2.699)	0.264		
VAT density, high vs low	2.601 (1.365–5.047)	0.004	3.468 (1.533–7.847)	0.003
VATI, high vs low	1.290 (0.690–2.424)	0.425		
VSR, high vs low	0.736 (0.391–1.377)	0.338		
IMAT area, large vs small	2.047 (1.091–3.887)	0.027	-	0.836
IMATI, high vs low	2.158 (1.149–4.107)	0.018	4.783 (2.058–11.112)	< 0.001
SM area, large vs small	0.457 (0.225–0.906)	0.027	0.295 (0.120–0.725)	0.008
SM density, high vs low	1.671 (0.891–3.159)	0.111		
SMI, high vs low	0.460 (0.241–0.866)	0.017	-	0.335

Abbreviations: *HCC* Hepatocellular carcinoma, *HBsAg* Hepatitis B surface Antigen, *AFP* Alpha fetoprotein, *TB* Total bilirubin, *SAT* Subcutaneous adipose tissue, *VAT* Visceral adipose tissue, *VATI* Visceral adipose tissue index, *VSR* Visceral to subcutaneous adipose tissue area ratio, *IMAT* Intramuscular adipose tissue, *IMATI* Intramuscular biopose tissue index, *SM* Skeletal muscle, *SMI* Skeletal muscle index
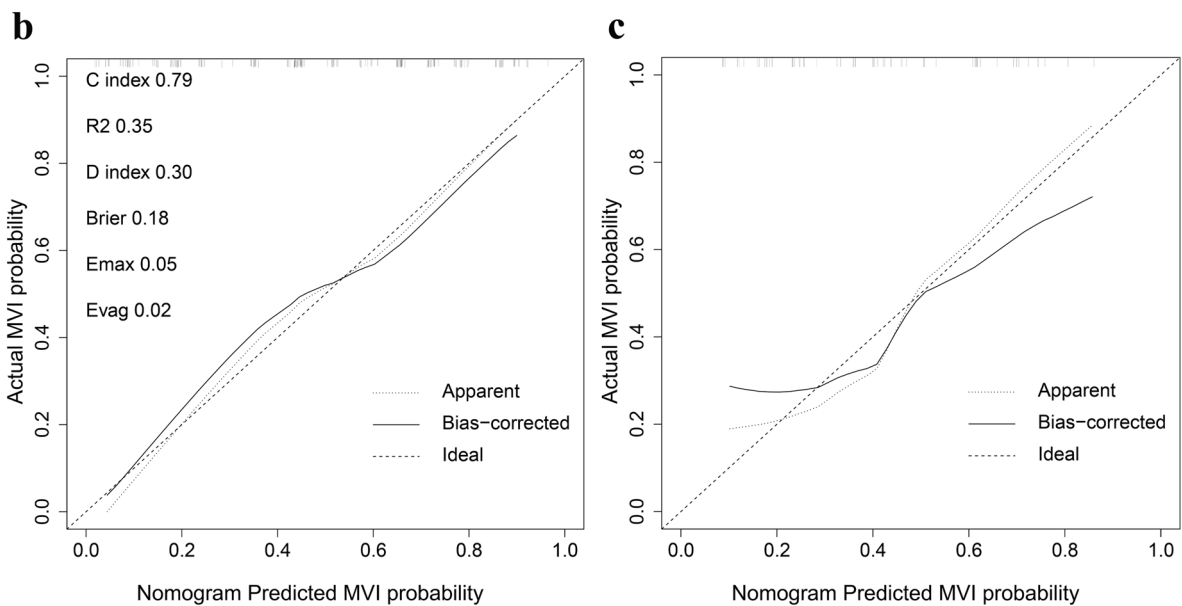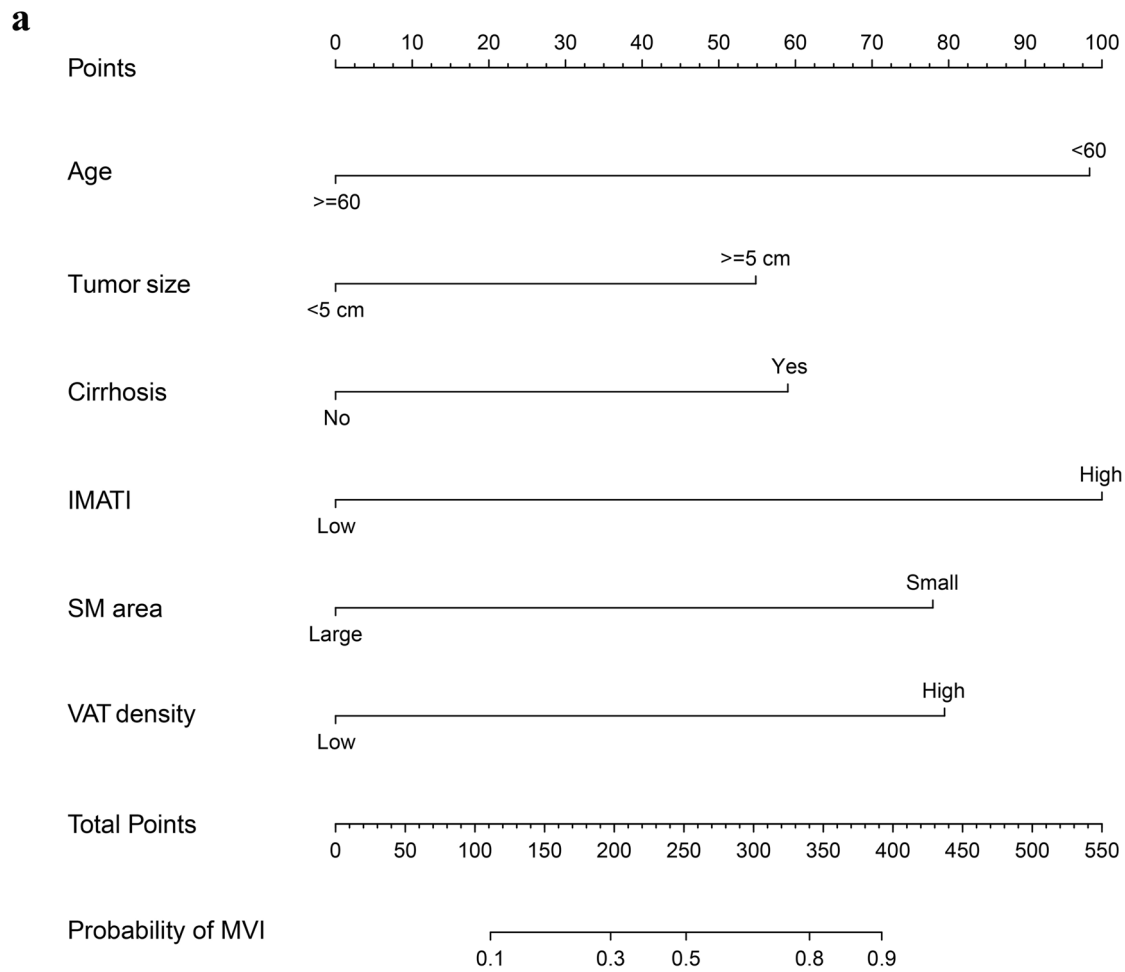
Fig. 3 Nomogram model for predicting MVI of HCC patients (**a**) and the calibration curve of the nomogram in training (**b**) and validation cohorts (**c**)

Table 3 The changes variables after 200 rounds of tenfold internal validation

Variable	Primary value	Calibration value	Change
C index	0.79	0.79	0
R^2	0.35	0.32	-0.03
D index	0.30	0.24	-0.06
Brier score	0.18	0.18	0
Emax	0.05	0.30	+0.25
Eavg	0.02	0.13	+0.11

Abbreviations: *C index* Concordance index, *D index* Discrimination index

resection methods or surgical margins had impact on recurrence and OS (Supplementary Figs. 3, 4).

In order to facilitate the clinical use of the nomogram, we have provided an online version accessible via the hyperlink: https://sdmxc.shinyapps.io/MVInom/. By setting variables greater than or equal to the cut-off value to 1 and those less than it to 0,

the predicted probability of MVI for patients can be quickly obtained.

Discussion

In the present study, we showed that adipose and muscle tissues-related variables, including VAT density, IMATI and SM area, were capable to serve as independent predictors for MVI. Furthermore, we incorporated the above variables with three common clinical variables (age, tumor size, cirrhosis) to develop an MVI-predicting model which exhibited good consistency and high accuracy. In the process of validating the clinical utility, our nomogram was also superior to the models only based on imaging or clinical variables. Compared with other radiomics nomograms [11, 12], we only need one plain CT image at L3 level for data extraction, without the need to conduct complex three-dimensional tumor target delineation at various phases of enhanced scanning, which will bring heavy computational burden. Recently, some researchers have employed liver biopsy specimens
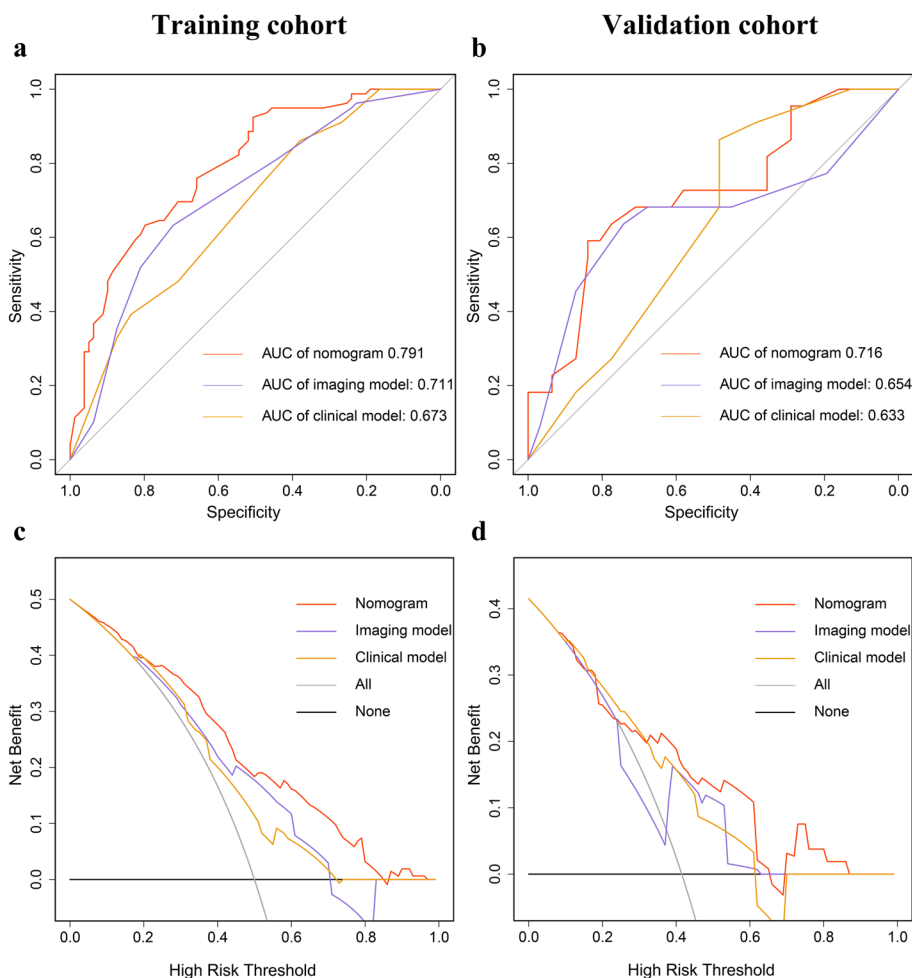

Fig. 4 ROC curve (**a**-**b**) and DCA (**c**-**d**) of the nomogram, imaging and clinical models in training and validation cohorts

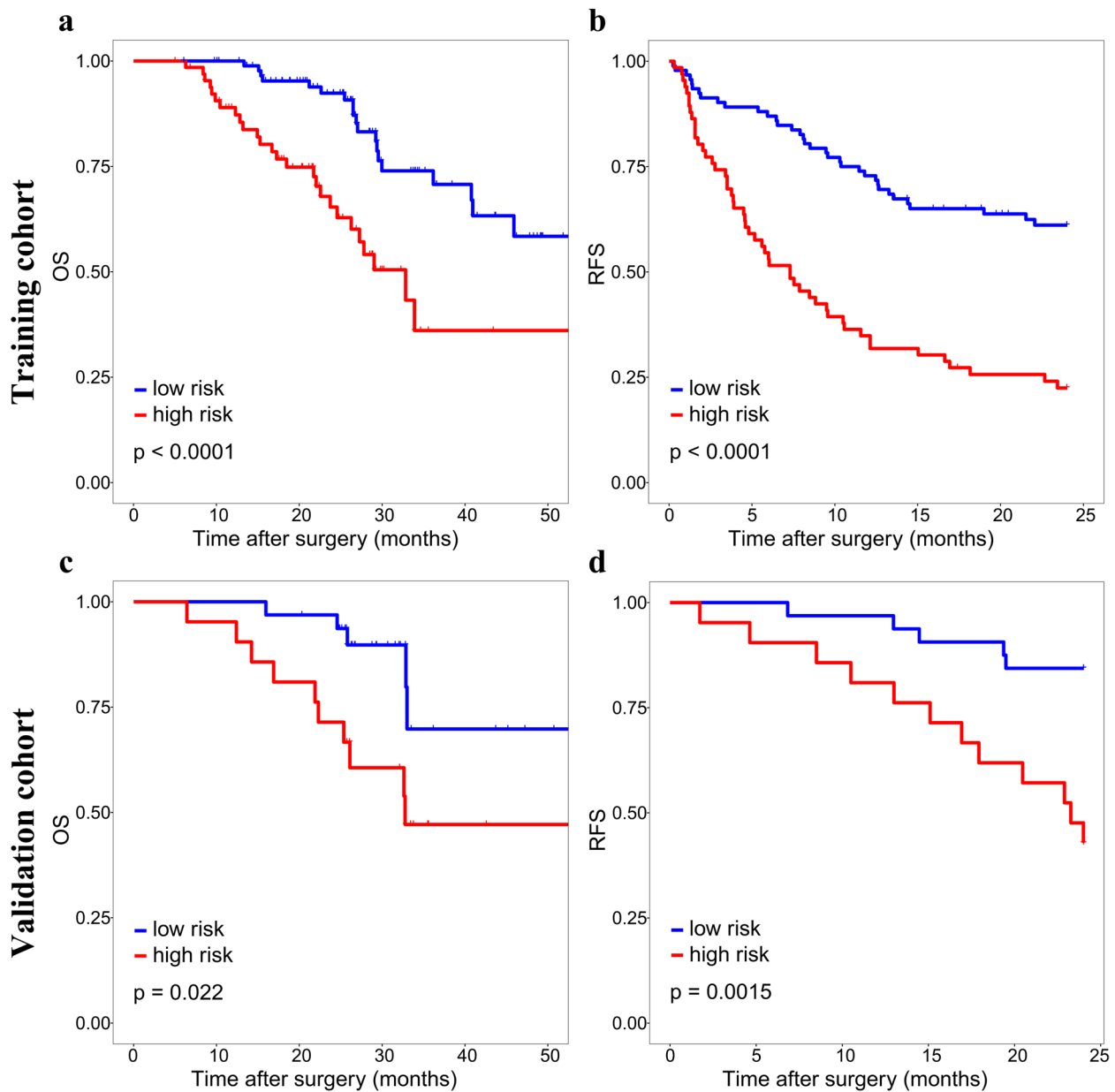Mao *et al. Biomarker Research*   (2023) 11:87

Page 11 of 16

Fig. 5 Kaplan–Meier curves of OS and 2-year RFS for patients with different risks scores in training cohort (**a**, **b**) and validation cohort (**c**, **d**)

to analyze gene expression or even radio-genomics for predicting MVI [31, 32]. Despite its good predictive performance, tissue biopsy for the diagnosis of HCC is unnecessary for patients with typical imaging findings according to some clinical guidelines [33, 34]. Additionally, invasive procedure may lead to potential risks such as tumor seeding and fatal bleeding, which outweigh the benefits [34, 35].

In the previously published MVI-predicting nomograms, tumor size, cirrhosis and age has been confirmed as risk factors for vascular invasion in HCC. Pawlik et al.

reported that the incidence of MVI was almost twice as high in tumors larger than 5 cm (61%) when compared to smaller tumors (32%), and it increased continuously with increasing tumor size [36]. Cirrhosis patients were frequently present with alterations in hemodynamic and blood microenvironment. On one hand, secondary hypersplenism could decrease platelet counts and reduce portal blood flow to the liver, which was conducive to the formation of MVI [10]. On the other hand, the increase of von Willebrand factor and other procoagulants, as well as the decrease in generation of antithrombin in patients
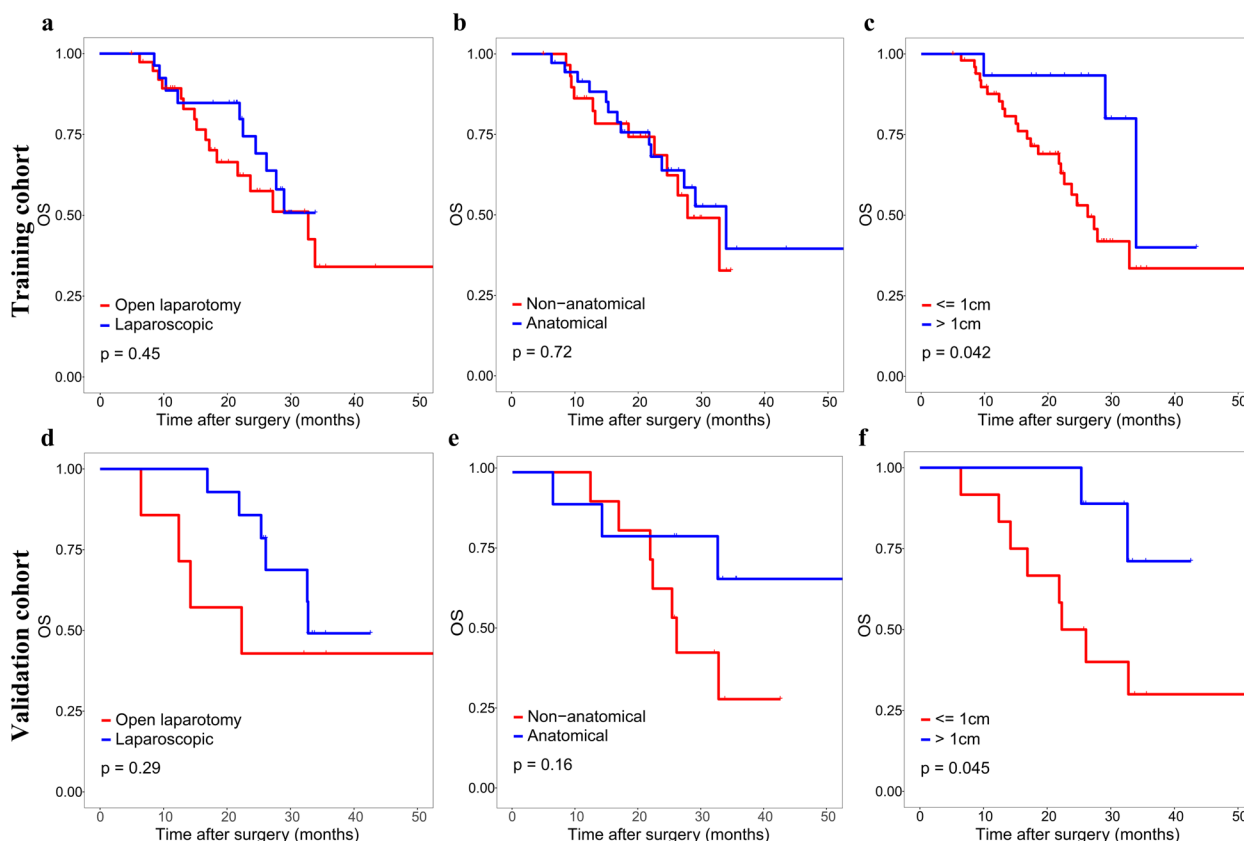
Fig. 6 Kaplan–Meier curves of OS for high-risk patients under different surgical approaches, resection methods and surgical margins in training cohort (**a**-**c**) and validation cohort (**d**-**f**)

with cirrhosis, could cause an imbalance in the coagulation and fibrinolytic systems [37, 38]. The mechanisms mentioned above could both serve as stimuli for thrombosis and vascular invasion. In current study, younger HCC patients had a higher incidence of MVI, which was in consistent with another research [12]. This observation might be attributed to the high aggressiveness of the tumor in young patients; however, the exact underlying mechanism remains to be investigated by future studies [39].

For body composition-related variables, metabolic theory could support our findings. Because most fatty acids in VAT are transported via the portal vein, higher degree of visceral obesity will expose the liver to high concentrations of fatty acids and glycerol. This, in turn, leads to a series of liver dysfunctions, such as reduced hepatic insulin extraction, increased hepatic glucose production, and ultimately results in type 2 diabetes and insulin resistance [40]. In addition, accumulation of visceral adipose is also linked with the upregulation of aquaporin adipose, an adipocyte-specific glycerol channel, leading to the increased glycerol secretion from VAT [41]. The liver-specific aquaporin protein AQP-9 could absorb excess glycerol and convert it into glycerol phosphate through glycerokinase, which is also one of the mechanisms leading to hyperglycemia [42]. Hyperglycemia alters the size and composition of the basement membranes in micro and large vessels, which in turn increase vascular permeability and fragility, and make it easier for tumors to invasion vascular and metastasize [43–45]. Furthermore, with continues accumulation of lipids, adipose tissues will undergo complex process of remodeling, and the secretion of adipokines, such as leptin, adiponectin, interleukin, vascular endothelial growth factor (VEGF), and hypoxia-inducible factor (HIF) will significantly increase [46], which could induce angiogenesis by stimulating endothelial cell proliferation, migration, and tube formation [47].

SM area provides information on changes in muscle structure, while IMAT indicates alterations in the content of intra- and inter-myocellular adipose [48]. The former parameter denotes muscle quantity and is served as an assessment metric for sarcopenia, and the latter parameter reflects muscle quality and is served as an evaluation index for myosteatosis [20]. Recent studies have established that sarcopenia is positively associated with
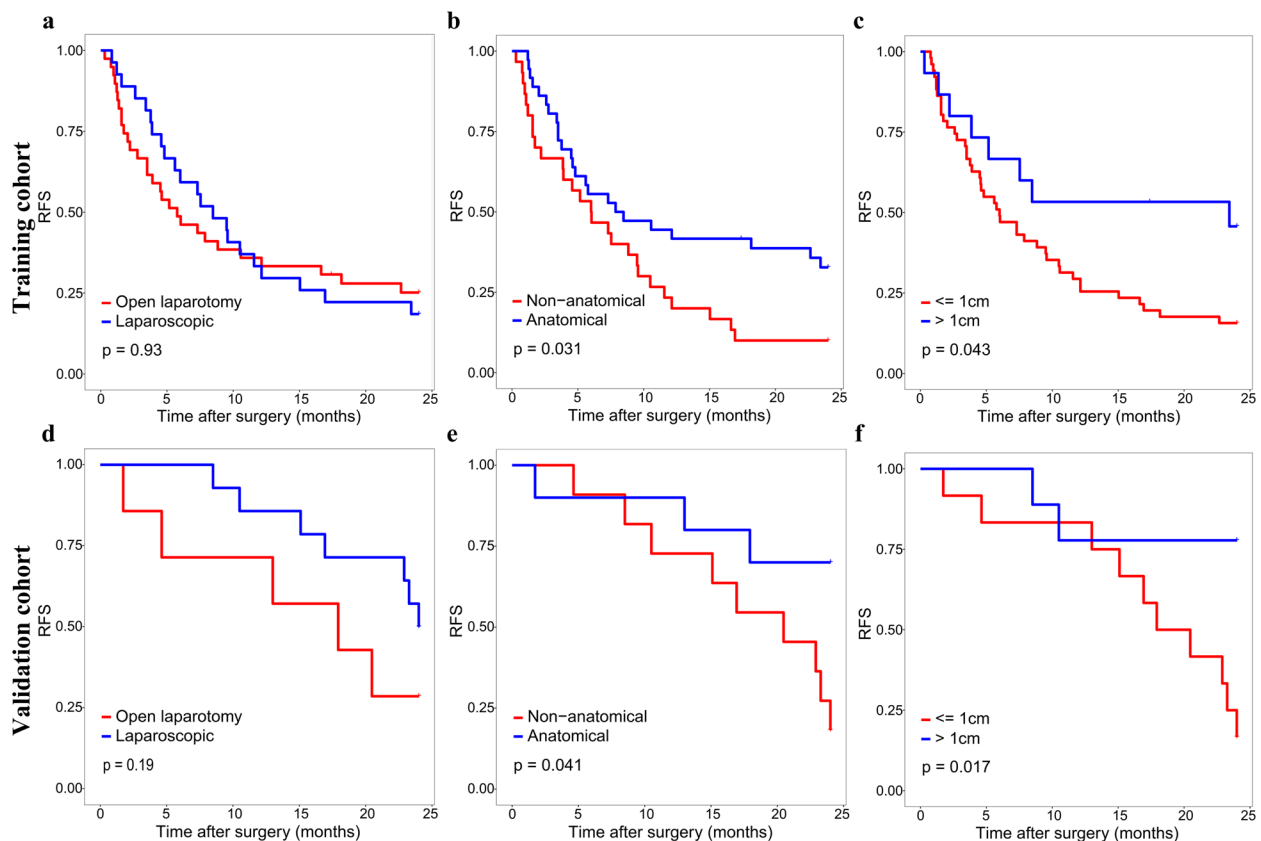
Fig. 7 Kaplan–Meier curves of 2-RFS for high-risk patients under different surgical approaches, resection methods and surgical margins in training cohort (**a**-**c**) and validation cohort (**d**-**f**)

evaluated all-cause mortality in HCC patients [49, 50]. Though the detailed mechanism has yet to be fully elucidated, however, there are two generally accepted hypotheses. Depletion of muscle could lead to a reduction in the secretion of specific cytokines, such as insulin-like growth factor (IGF)-1, which is associated with advanced clinicopathological variables of HCC [51, 52]. In addition, sarcopenia could also result in the impairment of certain protein hydrolysis systems, such as the tumor necrosis factor (TNF)-α system, thereby facilitating the process of tumor migration and invasion [53].

To date there have no studies that illuminate molecular mechanisms between myosteatosis and tumor angiogenesis. However, pathological changes in muscle have a strong correlation with chronic liver disease [54]. Montano-Loza et al. studied a cohort of cirrhotic patients undergoing liver transplant evaluation, in which the prevalence of muscular steatosis was greater than 50% [55]. In cirrhosis patients, the absorption of lipids and fat-soluble vitamins may be impacted as a result of several physiological changes, such as nausea, anorexia, increased intra-abdominal pressure, and impaired gut motility. Malnutrition promotes the catabolism of muscle

proteins, leading to depletion of muscle mass [56, 57]. In addition, chronic hepatic inflammation plays a significant role in promoting systemic inflammation, which in turn also accelerates the catabolism of muscle proteins [58]. There have been studies shown that liver disease not only triggers muscle atrophy and changes its structure, but the muscle in turn promotes the further development of liver disease [54, 59]. Therefore, there may exist an interaction between liver disease and muscle tissue, which exerts an influence on the IMAT, and consequently modulates the expression of downstream adipokines and myokines. Such a dynamic interaction and these cytokines may contribute to the tumor invasion and progression of liver disease.

There are several limitations in our study. Firstly, the limited number of patients impose inherent restrictions on our findings, thus larger external datasets are needed to validate and refine it. Secondly, a prospective study is required to further confirm the reliability of the nomogram. Thirdly, MVI grade was not taken into account in the MVI positive group. Fourthly, this nomogram model is constructed to predict the risk of MVI. Since macrovascular invasion is also a common phenomenon in HCC

Mao *et al. Biomarker Research*   (2023) 11:87

Page 14 of 16

and is known to be an important predictor of poor survival outcomes [60, 61], whether this nomogram model is fitted for the predication of macrovascular invasion in HCC deserves further study.

In addition, some baseline characteristics showed difference between the two cohorts, and it's inevitable as the process of data collection in these two hospitals were conducted independently. However, these differences had minimal impact on our results. Firstly, data selection and model construction were both performed within training cohort. Two hundred rounds of internal tenfold cross-validation method was used to verify the stable of our model, which could reduce overfitting of result and maximize the utilization of the data. Secondly, although split sample approach could create two cohorts with no differences [62], it could lead the model being unstable, that is, the performance evaluation was correlated with the partition of the training and validation cohorts. Different partitions might yield different estimates of the accuracy [14, 63]. Therefore, we chose original cohort distribution to ensure the randomness and independence of the data and increase generalizability of the model. In fact, we also verified our model by propensity score matching method to match the baseline characteristics data of the validation cohort and the training cohort, and it still demonstrated good predictive capability (data not shown). This suggests that our model has good generalizability and can be extrapolated to patients in other hospitals.

Conclusion

By combining 6 preoperative independently predictive factors of MVI, a nomogram is constructed. This model provides an optimal preoperative estimation of MVI risk in HCC patients. For patients with higher MVI scores, anatomical hepatectomy with wide margins may be recommend to reduce early recurrence and extend survival.

Abbreviations

AFP	Alpha-fetoprotein
ANN	Artificial neural network
BMI	Body mass index
C-index	Concordance index
CT	Computed tomography
DCA	Decision curve analysis
D index	Discrimination index
HCC	Hepatocellular carcinoma
HU	Hounsfield Unit
IMATI	Intramuscular adipose tissue index
IGF	Insulin-like growth factor
KM	Kaplan-Meier
LASSO	Least absolute shrinkage and selection operator
L3	Lumbar vertebra
MRI	Magnetic resonance imaging
MVI	Microvascular invasion
RFS	Recurrence free survival
ROC	Receiver operating characteristic
SM	Skeletal muscle
SMI	Skeletal muscle index
TACE	Transcatheter arterial chemoembolization
TNF	Tumor necrosis factor
VAR	Visceral to subcutaneous adipose tissue area ratio
VAT	Visceral adipose tissue
VEGF	Vascular endothelial growth factor

Supplementary Information

The online version contains supplementary material available at https://doi.org/10.1186/s40364-023-00527-z.

> **Additional file 1: Supplementary Figure 1.** Examples of muscle and adipose tissue measurements: (a) subcutaneous adipose area (b) skeletal muscle area; (c) visceral adipose area; (d) intra-muscular adipose tissue. **Supplementary Figure 2.** The optimal cut-off values of the nomogram scores. **Supplementary Figure 3.** Kaplan-Meier curves of OS for low-risk patients under different surgical approaches, resection methods and surgical margins in training cohort (a-c) and validation cohort (d-f). OS = overall survival. **Supplementary Figure 4.** Kaplan-Meier curves of 2-RFS for low-risk patients under different surgical approaches, resection methods and surgical margins in training cohort (a-c) and validation cohort (d-f). RFS = recurrence free survival. **Supplementary Table 1.** Cut-off values of body composition for male and female.

Availability of data and materials
All data and material analyzed during this study are included in this article/supplementary file. Further inquiries can be directed to the corresponding author.

Declarations

Ethics approval and consent to participate
This retrospective study was reviewed and approved by Institutional Review Board of Qilu hospital of Shandong university [approval number: 2021(222)].

Consent for publication
All authors have read and approved the manuscript and agree with submission to Biomarker Research.

Competing interests
The authors declare no competing interests.

Author details
[1]Department of General Surgery, Qilu Hospital, Shandong University, 107 West Wen Hua Road, Jinan 250012, China. [2]Department of Radiology, Qilu Hospital, Shandong University, Jinan, China. [3]Institute for Financial Studies, Shandong University, Jinan 250100, China.

References

1. Sung H, Ferlay J, Siegel RL, Laversanne M, Soerjomataram I, Jemal A, et al. Global cancer statistics 2020: GLOBOCAN estimates of incidence and mortality worldwide for 36 cancers in 185 countries. CA Cancer J Clin. 2021;71(3):209–49.
2. Li X, Han M, Zhang H, Liu F, Pan Y, Zhu J, et al. Structures and biological functions of zinc finger proteins and their roles in hepatocellular carcinoma. Biomark Res. 2022;10(1):2.
3. Roayaie S, Obeidat K, Sposito C, Mariani L, Bhoori S, Pellegrinelli A, et al. Resection of hepatocellular cancer ≤2 cm: results from two Western centers. Hepatology (Baltimore, MD). 2013;57(4):1426–35.
4. Rodríguez-Perálvarez M, Luong TV, Andreana L, Meyer T, Dhillon AP, Burroughs AK. A systematic review of microvascular invasion in hepatocellular carcinoma: diagnostic and prognostic variability. Ann Surg Oncol. 2013;20(1):325–39.
5. Lim KC, Chow PK, Allen JC, Chia GS, Lim M, Cheow PC, et al. Microvascular invasion is a better predictor of tumor recurrence and overall survival following surgical resection for hepatocellular carcinoma compared to the Milan criteria. Ann Surg. 2011;254(1):108–13.
6. Mazzaferro V, Llovet JM, Miceli R, Bhoori S, Schiavo M, Mariani L, et al. Predicting survival after liver transplantation in patients with hepatocellular carcinoma beyond the Milan criteria: a retrospective, exploratory analysis. Lancet Oncol. 2009;10(1):35–43.
7. Hirokawa F, Hayashi M, Miyamoto Y, Asakuma M, Shimizu T, Komeda K, et al. Outcomes and predictors of microvascular invasion of solitary hepatocellular carcinoma. Hepatol Res. 2014;44(8):846–53.
8. Cucchetti A, Piscaglia F, Grigioni AD, Ravaioli M, Cescon M, Zanello M, et al. Preoperative prediction of hepatocellular carcinoma tumour grade and micro-vascular invasion by means of artificial neural network: a pilot study. J Hepatol. 2010;52(6):880–8.
9. Shariat SF, Karakiewicz PI, Suardi N, Kattan MW. Comparison of nomograms with other methods for predicting outcomes in prostate cancer: a critical analysis of the literature. Clin Cancer Res. 2008;14(14):4400–7.
10. Lei Z, Li J, Wu D, Xia Y, Wang Q, Si A, et al. Nomogram for preoperative estimation of microvascular invasion risk in hepatitis B virus-related hepatocellular carcinoma within the Milan criteria. JAMA Surg. 2016;151(4):356–63.
11. Yang L, Gu D, Wei J, Yang C, Rao S, Wang W, et al. A radiomics nomogram for preoperative prediction of microvascular invasion in hepatocellular carcinoma. Liver Cancer. 2019;8(5):373–86.
12. Ma X, Wei J, Gu D, Zhu Y, Feng B, Liang M, et al. Preoperative radiomics nomogram for microvascular invasion prediction in hepatocellular carcinoma using contrast-enhanced CT. Eur Radiol. 2019;29(7):3595–605.
13. Steyerberg EW, Harrell FE Jr, Borsboom GJ, Eijkemans MJ, Vergouwe Y, Habbema JD. Internal validation of predictive models: efficiency of some procedures for logistic regression analysis. J Clin Epidemiol. 2001;54(8):774–81.
14. Simon R. Development and evaluation of therapeutically relevant predictive classifiers using gene expression profiling. J Natl Cancer Inst. 2006;98(17):1169–71.
15. Yang J, Chen K, Zheng C, Chen K, Lin J, Meng Q, et al. Impact of sarcopenia on outcomes of patients undergoing liver resection for hepatocellular carcinoma. J Cachexia Sarcopenia Muscle. 2022;13(5):2383–92.
16. Ebadi M, Dunichand-Hoedl AR, Rider E, Kneteman NM, Shapiro J, Bigam D, et al. Higher subcutaneous adipose tissue radiodensity is associated with increased mortality in patients with cirrhosis. JHEP Rep. 2022;4(7): 100495.
17. Radu P, Ebadi M, Montano-Loza AJ, Dufour JF. What is the role of body composition assessment in HCC management? Cancers. 2022;14(21):5290.
18. von Hessen L, Roumet M, Maurer MH, Lange N, Reeves H, Dufour JF, et al. High subcutaneous adipose tissue density correlates negatively with survival in patients with hepatocellular carcinoma. Liver Int. 2021;41(4):828–36.
19. Ohki T, Tateishi R, Shiina S, Goto E, Sato T, Nakagawa H, et al. Visceral fat accumulation is an independent risk factor for hepatocellular carcinoma recurrence after curative treatment in patients with suspected NASH. Gut. 2009;58(6):839–44.
20. Fujiwara N, Nakagawa H, Kudo Y, Tateishi R, Taguri M, Watadani T, et al. Sarcopenia, intramuscular fat deposition, and visceral adiposity independently predict the outcomes of hepatocellular carcinoma. J Hepatol. 2015;63(1):131–40.
21. Gallo P, Silletta M, De Vincentis A, Lo Prinzi F, Terracciani F, Di Fazio G, et al. Sarcopenia in hepatocellular carcinoma: pathogenesis and management. Chemotherapy. 2022;67(3):152–63.
22. Ebadi M, Bhanji RA, Mazurak VC, Montano-Loza AJ. Sarcopenia in cirrhosis: from pathogenesis to interventions. J Gastroenterol. 2019;54(10):845–59.
23. Arsenii N, Piardi T, Diébold MD, Chenard MP, Drame M, De Mestier L, et al. Impact of visceral obesity on microvascular invasion in hepatocellular carcinoma. Cancer Invest. 2016;34(6):271–8.
24. Wu Z, Lu H, Xie Q, Cheng J, Ma K, Hu X, et al. Preoperative assessment of abdominal adipose tissue to predict microvascular invasion in small hepatocellular carcinoma. J Clin Transl Hepatol. 2022;10(2):184–9.
25. Cong WM, Bu H, Chen J, Dong H, Zhu YY, Feng LH, et al. Practice guidelines for the pathological diagnosis of primary liver cancer: 2015 update. World J Gastroenterol. 2016;22(42):9279–87.
26. Wang D, Zhao J, Zhang R, Yan Q, Zhou L, Han X, et al. The value of CT radiomic in differentiating mycoplasma pneumoniae pneumonia from streptococcus pneumoniae pneumonia with similar consolidation in children under 5 years. Front Pediatr. 2022;10: 953399.
27. Pang G, Shao G, Zhao F, Liu C, Zhong H, Guo W. CT virtual endoscopy for analyzing variations in the hepatic portal vein. Surg Radiol Anat. 2015;37(5):457–62.
28. Shen W, Punyanitya M, Wang Z, Gallagher D, St-Onge MP, Albu J, et al. Total body skeletal muscle and adipose tissue volumes: estimation from a single abdominal cross-sectional image. J Appl Physiol (Bethesda, Md: 1985). 2004;97(6):2333–8.
29. Miller KD, Jones E, Yanovski JA, Shankar R, Feuerstein I, Falloon J. Visceral abdominal-fat accumulation associated with use of indinavir. Lancet (London, England). 1998;351(9106):871–5.
30. Mitsiopoulos N, Baumgartner RN, Heymsfield SB, Lyons W, Gallagher D, Ross R. Cadaver validation of skeletal muscle measurement by magnetic resonance imaging and computerized tomography. J Appl Physiol (Bethesda, Md : 1985). 1998;85(1):115–22.
31. Banerjee S, Wang DS, Kim HJ, Sirlin CB, Chan MG, Korn RL, et al. A computed tomography radiogenomic biomarker predicts microvascular invasion and clinical outcomes in hepatocellular carcinoma. Hepatology (Baltimore, MD). 2015;62(3):792–800.
32. Beaufrère A, Caruso S, Calderaro J, Poté N, Bijot JC, Couchy G, et al. Gene expression signature as a surrogate marker of microvascular invasion on routine hepatocellular carcinoma biopsies. J Hepatol. 2022;76(2):343–52.
33. Marrero JA, Ahn J, Rajender Reddy K. ACG clinical guideline: the diagnosis and management of focal liver lesions. Am J Gastroenterol. 2014;109(9):1328–47.
34. Tapper EB, Lok AS. Use of liver imaging and biopsy in clinical practice. N Engl J Med. 2017;377(8):756–68.
35. Ao H, Xin Z, Jian Z. Liquid biopsy to identify biomarkers for immunotherapy in hepatocellular carcinoma. Biomark Res. 2021;9(1):91.
36. Pawlik TM, Delman KA, Vauthey JN, Nagorney DM, Ng IO, Ikai I, et al. Tumor size predicts vascular invasion and histologic grade: Implications for selection of surgical treatment for hepatocellular carcinoma. Liver Transpl. 2005;11(9):1086–92.
37. Ferro D, Quintarelli C, Lattuada A, Leo R, Alessandroni M, Mannucci PM, et al. High plasma levels of von Willebrand factor as a marker of endothelial perturbation in cirrhosis: relationship to endotoxemia. Hepatology (Baltimore, MD). 1996;23(6):1377–83.
38. Carmassi F, Morale M, De Negri F, Carrai M. Modulation of hemostatic balance with antithrombin III replacement therapy in a case of liver cirrhosis associated with recurrent venous thrombosis. J Mol Med (Berl). 1995;73(2):89–93.
39. Wallington M, Saxon EB, Bomb M, Smittenaar R, Wickenden M, McPhail S, et al. 30-day mortality after systemic anticancer treatment for breast and lung cancer in England: a population-based, observational study. Lancet Oncol. 2016;17(9):1203–16.
40. Neeland IJ, Hughes C, Ayers CR, Malloy CR, Jin ES. Effects of visceral adiposity on glycerol pathways in gluconeogenesis. Metabolism. 2017;67:80–9.
41. Kishida K, Kuriyama H, Funahashi T, Shimomura I, Kihara S, Ouchi N, et al. Aquaporin adipose, a putative glycerol channel in adipocytes. J Biol Chem. 2000;275(27):20896–902.

Mao *et al. Biomarker Research*   (2023) 11:87

Page 16 of 16

42. Neeland IJ, Ross R, Després JP, Matsuzawa Y, Yamashita S, Shai I, et al. Visceral and ectopic fat, atherosclerosis, and cardiometabolic disease: a position statement. Lancet Diabetes Endocrinol. 2019;7(9):715–25.

43. Negrean M, Stirban A, Stratmann B, Gawlowski T, Horstmann T, Götting C, et al. Effects of low- and high-advanced glycation endproduct meals on macro- and microvascular endothelial function and oxidative stress in patients with type 2 diabetes mellitus. Am J Clin Nutr. 2007;85(5):1236–43.

44. Wautier JL, Zoukourian C, Chappey O, Wautier MP, Guillausseau PJ, Cao R, et al. Receptor-mediated endothelial cell dysfunction in diabetic vasculopathy. Soluble receptor for advanced glycation end products blocks hyperpermeability in diabetic rats. J Clin Invest. 1996;97(1):238–43.

45. Morss AS, Edelman ER. Glucose modulates basement membrane fibroblast growth factor-2 via alterations in endothelial cell permeability. J Biol Chem. 2007;282(19):14635–44.

46. Sun K, Kusminski CM, Scherer PE. Adipose tissue remodeling and obesity. J Clin Investig. 2011;121(6):2094–101.

47. Apte RS, Chen DS, Ferrara N. VEGF in signaling and disease: beyond discovery and development. Cell. 2019;176(6):1248–64.

48   Meister FA, Lurje G, Verhoeven S, Wiltberger G, Heij L, Liu WJ, et al. The role of sarcopenia and myosteatosis in short- and long-term outcomes following curative-intent surgery for hepatocellular carcinoma in a European cohort. Cancers. 2022;14(3):720.

49. Chang KV, Chen JD, Wu WT, Huang KC, Hsu CT, Han DS. Association between loss of skeletal muscle mass and mortality and tumor recurrence in hepatocellular carcinoma: a systematic review and meta-analysis. Liver Cancer. 2018;7(1):90–103.

50. Tantai X, Liu Y, Yeo YH, Praktiknjo M, Mauro E, Hamaguchi Y, et al. Effect of sarcopenia on survival in patients with cirrhosis: a meta-analysis. J Hepatol. 2022;76(3):588–99.

51. Peake JM, Della Gatta P, Suzuki K, Nieman DC. Cytokine expression and secretion by skeletal muscle cells: regulatory mechanisms and exercise effects. Exerc Immunol Rev. 2015;21:8–25.

52. Elmashad N, Ibrahim WS, Mayah WW, Farouk M, Ali LA, Taha A, et al. Predictive value of serum insulin-like growth factor-1 in hepatocellular carcinoma. Asian Pac J Cancer Prev. 2015;16(2):613–9.

53. Sachdeva M, Chawla YK, Arora SK. Immunology of hepatocellular carcinoma. World J Hepatol. 2015;7(17):2080–90.

54   Nachit M, Leclercq IA. Emerging awareness on the importance of skeletal muscle in liver diseases: time to dig deeper into mechanisms! Clin Sci (Lond). 2019;133(3):465–81.

55. Montano-Loza AJ, Angulo P, Meza-Junco J, Prado CM, Sawyer MB, Beaumont C, et al. Sarcopenic obesity and myosteatosis are associated with higher mortality in patients with cirrhosis. J Cachexia Sarcopenia Muscle. 2016;7(2):126–35.

56. Thandassery RB, Montano-Loza AJ. Role of Nutrition and Muscle in Cirrhosis. Curr Treat Options Gastroenterol. 2016;14(2):257–73.

57. Dasarathy S, Merli M. Sarcopenia from mechanism to diagnosis and treatment in liver disease. J Hepatol. 2016;65(6):1232–44.

58. Pérez-Baos S, Prieto-Potin I, Román-Blas JA, Sánchez-Pernaute O, Largo R, Herrero-Beaumont G. Mediators and patterns of muscle loss in chronic systemic inflammation. Front Physiol. 2018;9:409.

59. Eslamparast T, Montano-Loza AJ, Raman M, Tandon P. Sarcopenic obesity in cirrhosis-The confluence of 2 prognostic titans. Liver Int. 2018;38(10):1706–11.

60. Costentin CE, Ferrone CR, Arellano RS, Ganguli S, Hong TS, Zhu AX. Hepatocellular carcinoma with macrovascular invasion: defining the optimal treatment strategy. Liver Cancer. 2017;6(4):360–74.

61. Huang C, Zhu XD, Shen YH, Wu D, Ji Y, Ge NL, et al. Organ specific responses to first-line lenvatinib plus anti-PD-1 antibodies in patients with unresectable hepatocellular carcinoma: a retrospective analysis. Biomarker Res. 2021;9(1):19.

62. Shen J, Zhou Y, Yu B, Zhao K, Ding Y. Construction and validation of a nomogram for patients with multiple hepatocellular carcinoma: A SEER-based study. Eur J Surg Oncol. 2023;49(10):106966.

63. Steyerberg EW, Harrell FE Jr. Prediction models need appropriate internal, internal-external, and external validation. J Clin Epidemiol. 2016;69:245–7.

Publisher's Note